Science of the Total Environment 772 (2021) 145542

Contents lists available at ScienceDirect

Science of the Total Environment

journal homepage: www.elsevier.com/locate/scitotenv

Tracing riverine dissolved organic carbon and its transport to the halocline layer in the Chukchi Sea (western Arctic Ocean) using humic-like fluorescence fingerprinting

Jinyoung Jung [a,1], Jin Eui Son [a,b,1], Yun Kyung Lee [b], Kyoung-Ho Cho [a], Youngju Lee [a], Eun Jin Yang [a], Sung-Ho Kang [a], Jin Hur [b,*]

[a] Division of Ocean Sciences, Korea Polar Research Institute, 26, Songdomirae-ro, Yeonsu-gu, Incheon 21990, Republic of Korea
[b] Department of Environment & Energy, 209, Neungdong-ro, Gwangjin-gu, Sejong University, Seoul 05006, Republic of Korea

HIGHLIGHTS

- Spatial distributions of DOC and humic-like FDOM were examined in the Chukchi Sea.
- DOC in river runoff and f_{river} from $\delta^{18}O$ were used to estimate riverine DOC.
- Characteristic of DOM fluorescence was a powerful means to trace riverine DOM.
- Sea-ice formation is a key mechanism for carrying riverine DOM to the deep layer.

GRAPHICAL ABSTRACT

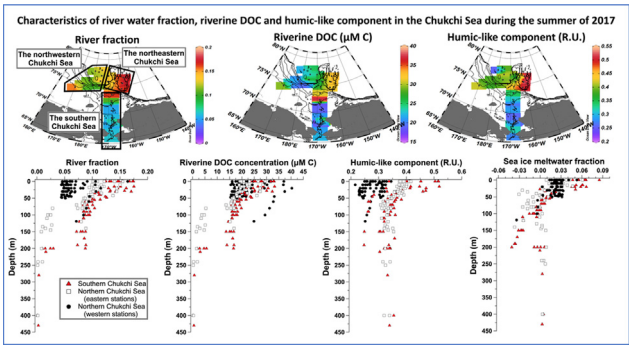

ARTICLE INFO

Article history:
Received 3 November 2020
Received in revised form 26 January 2021
Accepted 27 January 2021
Available online 3 February 2021

Editor: Ashantha Goonetilleke

Keywords:
Riverine DOC
Humic-like fluorescence
River water
Chukchi Sea
Western Arctic

ABSTRACT

Dissolved organic carbon (DOC) and the fluorescence properties of dissolved organic matter (FDOM) were investigated using parallel factor analysis (PARAFAC) for seawater samples collected in the Chukchi Sea (65°N–78°N, 170°E–160°W) during summer 2017. River water (f_{river}) and sea-ice meltwater ($f_{sea\ ice\ melt}$) fractions were also derived using oxygen isotopes ratios ($\delta^{18}O$) to examine the influence of sea ice on riverine DOM. The spatial distributions of f_{river}, riverine DOC, and the humic-like fluorescent component (C1) showed an overall south-north gradient, with higher values in the northern Chukchi Sea in summer. Pronounced accumulation of river water and riverine DOM was also observed in the anticyclonic Beaufort Gyre at the eastern stations of the northern Chukchi Sea in association with a long water residence time. Estimated riverine DOC in the surface layer accounted for 27 ± 9% (range: 17–47%) of the total DOC in the southern Chukchi Sea, and 39 ± 6% (range: 32–49%) and 31 ± 4% (range: 25–37%) for the eastern and western stations of the northern Chukchi Sea, respectively. Humic-like C1 showed negative and positive relationships with sea-ice meltwater-corrected salinity ($S_{sim\_corrected}$) and f_{river}, respectively. However, Arctic river waters with distinct humic-like C1 characteristics were likely mixed in the northern Chukchi Sea. The vertical distributions of riverine DOC, humic-like C1 fluorescence, and f_{river} generally decreased with water depth, reflecting the strong influence of riverine DOM in the surface layer. Although riverine DOM and f_{river} were dominant in the upper 50 m of the water column, they were also pronounced in the upper halocline (50–200 m), in which $f_{sea\ ice\ melt}$ dropped below zero. Our results indicated the existence of brine rejected from growing sea ice, and that sea-ice formation was a key factor for the transport of riverine DOM to the upper halocline layer in the northern Chukchi Sea.

* Corresponding author.
E-mail address: jinhur@sejong.ac.kr (J. Hur).
[1] These authors contributed equally to this work.

https://doi.org/10.1016/j.scitotenv.2021.145542
0048-9697/

1. Introduction

The Arctic Ocean is currently experiencing rapid environmental and climate changes including accelerated warming (Overland et al., 2019), a decline in sea ice coverage (Cavalieri and Parkinson, 2012; Perovich et al., 2020), and increases in riverine discharge (Peterson et al., 2002; Holmes et al., 2018). In particular, massive inputs of river water make the influence of terrigenous dissolved organic matter (or carbon) (DOM or DOC) stronger in the Arctic Ocean than in other ocean basins (Guéguen et al., 2007; Holmes et al., 2012; Goncalves-Araujo et al., 2016); the Arctic Ocean receives approximately 10% of the global river discharge while accounting for only ~1% of the global ocean volume (McClelland et al., 2012). Furthermore, increasing air temperatures in the Arctic lead to permafrost thaw (Romanovsky et al., 2010; Schuur et al., 2015; Turetsky et al., 2020), which in turn will likely result in increases in terrigenous DOM output to surface waters of the Arctic Ocean (Frey and McClelland, 2009; Abbott et al., 2014; Le Fouest et al., 2018). The pan-Arctic flux of riverine DOC to the Arctic Ocean is estimated to be 25–36 Tg C yr^{-1} (Raymond et al., 2007; Manizza et al., 2009; McGuire et al., 2009; Holmes et al., 2012), suggesting a strong influence of riverine DOC supply on the Arctic Ocean. Understanding the fate of terrigenous DOC in the Arctic Ocean is a critical, as increased riverine DOC input could have profound impacts on the global carbon cycle as well as the marine carbon and biogeochemical cycles in the Arctic Ocean (Hansell et al., 2004; Cooper et al., 2005; Bates and Mathis, 2009; McGuire et al., 2009; Schaefer et al., 2014).

The biodegradability of riverine DOC is still debated. While some studies reported low biodegradability of riverine DOC (e.g., Lobbes et al., 2000; Dittmar and Kattner, 2003), other studies revealed that the biodegradability of Arctic riverine DOC varies seasonally from <10 to 40% with highest biodegradability typically during snowmelt due to rapid transport across frozen soil (e.g., Holmes et al., 2008; Mann et al., 2012; Wickland et al., 2012). These discrepancies in the dynamics of riverine DOC can be explained by seasonality, differences in the terrigenous DOC composition and regional hydrology, and residence time on the continental shelf (Holmes et al., 2008; Tanaka et al., 2016). In addition, recent studies reported that DOC in the cryospheric components, such as permafrost and snow, could be largely biodegradable (e.g., Abbott et al., 2014; Gao et al., 2019; Zhang et al., 2020), suggesting that a larger proportion of DOC in the cryospheric components may be released to Arctic rivers and ultimately to the Arctic Ocean by a warming climate and permafrost thaw (Frey and McClelland, 2009).

In the western Arctic Ocean, significant removal of riverine DOC was reported during transport across the ocean shelf (Cooper et al., 2005) and within the Beaufort Gyre (Hansell et al., 2004). Manizza et al. (2009) simulated the spatial distribution and fate of riverine DOC in the Arctic, and reported that their model results for riverine DOC over predicted measured DOC without considering sinks for a fraction of riverine DOC. This indicates that conservative mixing (i.e., changes in DOC that follow changes in salinity) alone is insufficient to explain the distribution of riverine DOC. Microbial and photochemical degradation processes have been suggested as possible explanations for DOC removal in the Arctic Ocean (Hansell et al., 2004; Jørgensen et al., 2015). In addition, the transport of DOM to deep layers during sea-ice formation has been studied (Guéguen et al., 2007; Stedmon et al., 2011a). However, the influences of sea-ice formation and subsequent ice melt on DOM distribution have not yet been fully clarified. For example, some studies in the Chukchi Sea have reported that sea-ice meltwater influences DOM via dilution (Mathis et al., 2005, 2007; Logvinova et al., 2016). Yet, in contrast, a high abundance of terrigenous material was observed in sea ice over the Chukchi and Beaufort Sea shelves (Eicken et al., 2005), suggesting the potential for increasing DOM concentrations with sea-ice melting (Shen et al., 2016). Given the changes in Arctic sea ice regimes (i.e., reduced summer minimum ice extent (Cavalieri and Parkinson, 2012), ice thinning (Kwok et al., 2009), and the reduction in multi-year ice extent (Comiso, 2012)), further studies are required to understand the processes of DOM production and removal during sea-ice formation and melting.

The optical properties of chromophoric DOM (CDOM), and particularly its fluorescence properties (FDOM), have proven to be useful tracers for Arctic riverine inputs (e.g., Walker et al., 2013; Drozdova et al., 2017, 2018) and as proxies for the physical mixing of Arctic water masses (e.g., Goncalves-Araujo et al., 2016; Tanaka et al., 2016). This is because they provide not only quantitative information on DOM but also qualitative information regarding its composition and origin (Coble, 1996, 2007; Coble et al., 1998). Considerable effort has been devoted to investigating the optical properties of DOM to improve understanding of biogeochemical carbon cycles in various oceanic regions, which have primarily distinguished between terrestrial and marine DOM sources (e.g., Stedmon et al., 2003; Guéguen et al., 2012; Yamashita et al., 2015; Goncalves-Araujo et al., 2016; Mann et al., 2016; Tanaka et al., 2016; Chen et al., 2017, 2018; Le Fouest et al., 2018; Brogi et al., 2019). However, currently, there is a limited amount of data available on the spatial distribution and characteristics of riverine DOM in the western Arctic, especially the northwestern Chukchi Sea, due to limited observations.

In this study, we investigated the spatial distributions of DOC and the optical properties of FDOM in seawater samples collected in the Chukchi Sea during the summer of 2017. Our main objectives were to (1) estimate riverine DOC concentrations, (2) trace the mixing of riverine DOM using the optical properties of FDOM, and (3) investigate the influence of sea ice on the distribution of riverine DOM in the Chukchi Sea. To achieve these objectives, we also used oxygen isotope ratios ($\delta^{18}O$) to assess the relative fractions of river water (f_{river}) and sea-ice meltwater ($f_{sea\ ice\ melt}$). In doing so, we provide valuable new insight into the spatial distribution of riverine DOM to address a key data gap, especially for the northwestern Chukchi Sea.

2. Materials and methods

2.1. Field sampling

A hydrographic survey and seawater sampling were carried out at 32 stations in the Chukchi Sea aboard the Korean icebreaker IBR/V *Araon* during the ARA08B cruise (August 6–25, 2017) using a conductivity-temperature-depth (CTD) and rosette system holding 24 10-L Niskin bottles (SeaBird Electronics, SBE 911 plus) (Fig. 1). To facilitate data interpretation, the study area was geographically divided into three regions: the southern Chukchi Sea (stations 1–12, and 14), the northeastern Chukchi Sea (stations 15, 16, 27–30, and 33–35), and the northwestern Chukchi Sea (stations 17–26).

Seawater samples for DOC and FDOM were drawn from the Niskin bottles by gravity filtration through an inline pre-combusted (at 550 °C for 6 h) Whatman GF/F filter held in an acid-cleaned (0.1 M HCl) polycarbonate 47-mm filter holder (PP-47, ADVANTEC) (Chen et al., 2018). In each case, the filter holder was attached directly to the Niskin bottle spigot. The filtrate was then collected in an acid-cleaned glass bottle and distributed into two pre-combusted 20-mL glass ampoules with a sterilized serological pipette. Each ampoule was sealed with a torch, quick-frozen, and preserved at −24 °C until the analysis in the laboratory.

For the determination of $\delta^{18}O$, seawater samples were collected using the same method as for DOC and FDOM sampling. For each sample, the filtrate was placed in an acid-cleaned 20-mL glass vial, sealed with Parafilm, and stored at 4 °C until analysis.

2.2. Dissolved organic carbon measurement

DOC analysis was performed by high-temperature combustion using a Shimadzu TOC-L analyzer. Milli-Q water (blank) and consensus reference materials (CRM, 42–45 μM C for DOC, deep Florida Strait water

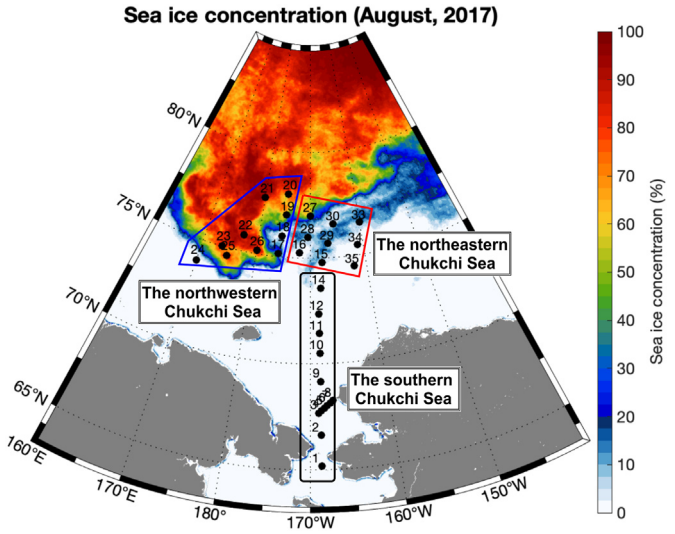

Fig. 1. Hydrographic survey locations in the Chukchi Sea. The locations and the numbers of the sampling stations are superimposed onto the mean sea ice concentrations derived from Advanced Microwave Scanning Radiometer (AMSR) 2 sea ice concentration data for August 2017. Geographic locations are divided into three regions: the southern Chukchi Sea (stations 1–12 and 14 enclosed by black lines), the northeastern Chukchi Sea (stations 15, 16, 27–30, and 33–35 enclosed by red lines), and the northwestern Chukchi Sea (stations 17–26 enclosed by blue lines). (For interpretation of the references to colour in this figure legend, the reader is referred to the web version of this article.)

obtained from University of Miami) were measured every sixth analysis to check the accuracy of the measurements. Analytical errors based on repeated measurements (at least three measurements per sample) were within 5% for DOC (Chen et al., 2018).

2.3. Optical measurements and excitation-emission matrices coupled with parallel factor analysis

Absorption spectra were obtained from 240 to 800 nm using a Shimadzu 1800 ultraviolet-visible (UV–Vis) spectrophotometer (Shimadzu Inc.). Three-dimensional fluorescence excitation-emission matrices (EEMs) were scanned using a Hitachi F-7000 luminescence spectrometer (Hitachi Inc.) at excitation/emission (Ex/Em) wavelengths of 250–500 nm/280–550 nm. The scanning steps for the Ex and Em wavelengths were set at 5 nm and 1 nm, respectively. The UV–Vis spectra were used for inner filter correction according to McKnight et al. (2001). Further details on the EEM measurements and the post-acquisition corrections are available in the published literature (Chen et al., 2010, 2017, 2018). The procedure for Raman unit (R.U.) normalization can also be found elsewhere (Lawaetz and Stedmon, 2009). Parallel factor (PARAFAC) modeling was performed using MATLAB 7.0.4, using the DOMFluor toolbox (Stedmon and Bro, 2008). Corrected EEMs of seawater samples were used for modeling. The number of fluorescent components was determined based on split-half validation and core consistency.

2.4. Stable oxygen isotope ratios measurement

$\delta^{18}O$ samples were analyzed by equilibration with carbon dioxide. Measurements were carried out with a stable isotope ratio mass spectrometer (Isoprime, Micromass, Manchester, UK) interfaced with a MultiPrep at Korea Basic Science Institute. The results are reported in the standard delta notation, where $\delta^{18}O = [(^{18}O/^{16}O_{sample}/^{18}O/^{16}O_{V\text{-}SMOW}) - 1] \times 1000$ (V-SMOW is Vienna-Standard Mean Ocean Water). The precision, based on repeated measurements of an internal standard, was determined to be <0.1‰.

2.5. Calculations

2.5.1. Freshwater components

$\delta^{18}O$ and salinity were used to determine the fractions of seawater ($f_{seawater}$), $f_{sea\ ice\ melt}$, and f_{river} in the collected samples following the approach of Mathis et al. (2007). Assuming that the water samples collected in our study area are a mixture of river water, sea-ice meltwater, and seawater, these respective fractions were calculated using the following mass balance equations:

$$f_{river} + f_{sea\ ice\ melt} + f_{seawater} = 1 \quad (1)$$

$$f_{river} \times \delta^{18}O_{river} + f_{sea\ ice\ melt} \times \delta^{18}O_{sea\ ice\ melt} + f_{seawater} \times \delta^{18}O_{seawater} = \delta^{18}O_{ob} \quad (2)$$

$$f_{river} \times S_{river} + f_{sea\ ice\ melt} \times S_{sea\ ice\ melt} + f_{seawater} \times S_{seawater} = S_{ob} \quad (3)$$

where f and S refer to the fraction and salinity, respectively; and $\delta^{18}O_{ob}$ and S_{ob} are the observed values from each seawater sample. Sea-ice formation, which drains brine into the underlying seawater, is represented by a negative $f_{sea\ ice\ melt}$ (Yamamoto-Kawai et al., 2008). The $\delta^{18}O$ and S values for the three end-members used in the calculations are summarized in Table 1, together with observed data by previous studies. The values of $\delta^{18}O_{seawater}$ and $S_{seawater}$ are taken from Mathis et al. (2007), Yamamoto-Kawai et al. (2008), and Logvinova et al. (2016). The average $\delta^{18}O$ value of river water in the Arctic Ocean is about −20‰ (Bauch, 1995; Cooper et al., 2008) and is applied as river water end-member in this study. $S_{sea\ ice\ melt}$ is from Ekwurzel et al. (2007) and Mathis et al. (2007), and $\delta^{18}O_{sea\ ice\ melt}$ is set to be −2‰ to represent the $\delta^{18}O$ value of sea ice in the western Arctic (Eicken et al., 2002; Pfirman et al., 2004; Mathis et al., 2007). The uncertainties of f_{river}, $f_{sea\ ice\ melt}$, and $f_{seawater}$, due to uncertainties in the range of end-member S and $\delta^{18}O$ data (Table 1), remain on average within ±0.01.

2.5.2. Riverine dissolved organic carbon

To estimate riverine DOC inputs, we followed the approach of Mathis et al. (2007). The riverine DOC concentration (μM C) was determined using the following equation:

$$\text{Riverine DOC} = f_{river} \times DOC_{river} \quad (4)$$

where DOC_{river} refers to the initial DOC concentration in river runoff. Cooper et al. (2008) reported that average DOC concentration measured at the river mouth of the Yukon River from 2003 to 2006 was 388 ± 84 μM C. In this study, a concentration of 350 μM C was used for the DOC_{river} concentration in the southern Chukchi Sea (i.e., stations 1–12 and 14), which is consistent with long-term observations in the Yukon River (Mathis et al., 2007). The uncertainty of riverine DOC in the southern Chukchi Sea, due to uncertainties in the range of DOC_{river} (i.e., 388 ± 84 μM C), was estimated to be ±3.9 μM C. For the northern Chukchi Sea, a value of 190 ± 10 μM C was taken as representative of the terrigenous DOC concentration, which corresponded to the zero-salinity (100% river water) DOC value from a plot of DOC versus sea-ice meltwater-corrected S in the region during the cruise. Further details on the relationship between DOC and sea-ice meltwater-corrected S are described in Section 3.3. The uncertainty of riverine DOC in the northern

Table 1
End-member values used in mass balance calculations[a].

End-member	Salinity (psu)	$\delta^{18}O$ (‰)
River water (f_{river})	0	−20 ± 1.0
Sea-ice meltwater ($f_{sea\ ice\ melt}$)	4 ± 1.0	−2 ± 1.0
Seawater ($f_{seawater}$)	34.8 ± 0.1	0.28 ± 0.03

[a] For further explanation see text in Section 2.5.1.

Chukchi Sea, due to uncertainties in the range of DOC_{river} (i.e., 190 ± 10 μM C), was estimated to be ±0.65 μM C.

3. Results and discussion

3.1. Spatial distributions of river water and sea-ice meltwater

The spatial distributions of sea surface salinity (SSS), temperature (SST), f_{river}, and $f_{sea\ ice\ melt}$ in the surface layer showed an overall south-north gradient (Fig. 2). The southern Chukchi Sea (i.e., stations 1–12 and 14) was characterized by high SSS and SST values, ranging from 27.7 to 32.8 psu and 7 to 11 °C, respectively (Fig. 2a and b). This indicates that warm and saline Pacific-origin waters flow into the Arctic Ocean through the Bering Strait (Woodgate et al., 2005). On the other hand, low values of f_{river} and $f_{sea\ ice\ melt}$ were observed in the southern Chukchi Sea, which ranged from 0.046 to 0.16 and 0.013 to 0.053, respectively, due to the strong influence of Pacific-origin waters (Fig. 2c and d). In contrast, the SSS and SST values sharply decreased in the northern Chukchi Sea, whereas both f_{river} and $f_{sea\ ice\ melt}$ increased, suggesting strong influences of river runoff and sea-ice meltwater.

The SSS, SST, f_{river}, and $f_{sea\ ice\ melt}$ in the northern Chukchi Sea showed an east-west gradient. Overall, the SST, f_{river} and $f_{sea\ ice\ melt}$ values were higher in the eastern stations (i.e., stations 15, 16, 27–30, and 33–35) than those in the western stations (i.e., stations 17–26). In contrast, SSS showed the opposite trend. The lowest values of SSS, ranging from 26.6 to 29.0 psu, were observed in the eastern stations where f_{river} and $f_{sea\ ice\ melt}$ varied from 0.12 to 0.17 and 0.05 to 0.09, respectively. On the other hand, in the western stations, the SSS ranged from 28.8 to 30.6 psu while f_{river} and $f_{sea\ ice\ melt}$ varied from 0.10 to 0.15 and 0.009 to 0.06, respectively. f_{river} was higher than $f_{sea\ ice\ melt}$ at all stations in the northern Chukchi Sea, indicating that river water is the main source of freshwater in the surface layer even in mid-late summer when extensive sea-ice melt occurs. In addition, the higher f_{river} and $f_{sea\ ice\ melt}$ values at the eastern stations coincided with the low SSS and elevated SST values (Fig. 2a and b), as well as an absence of sea ice (Fig. 1). This suggests that both river water and sea-ice meltwater make substantial contributions to the surface freshening in the eastern stations, and that the input of river water enhances sea-ice melt through increased heat input to the surface layer (either directly or indirectly) by stabilizing the upper ocean (Macdonald et al., 1999; Yamamoto-Kawai et al., 2009).

The $\delta^{18}O$ values of Arctic Ocean seawater are normally well correlated with S, particularly in areas with significant river runoff (Cooper et al., 2005). The relationship between $\delta^{18}O$ and S was influenced by sea-ice meltwater and brine (Fig. S1 and Table S1). We assumed the endpoints were seawater with a S of 34.8 and $\delta^{18}O$ value of 0.28‰ and river runoff with a $\delta^{18}O$ value of −20‰ and S of zero (Table 1). Data falling to the left of this presumed conservative mixing line in Fig. S1 indicate the mixing with sea-ice meltwater, whereas values falling to the right of the conservative mixing line indicate the influence of brine generated during sea-ice formation. It was clear that sea-ice meltwater was a significant component of surface waters (i.e., S < 30 psu) in the eastern stations where sea ice coverage was largely absent (Figs. 1 and S1). Although the influences of sea-ice meltwater and brine were observed, the relationship between $\delta^{18}O$ and S was not largely deviated from the conservative mixing line, suggesting that the influence of river runoff overwhelmed that of sea-ice meltwater and that river runoff is the main source of freshwater in our study region. However, it is worth noting that $\delta^{18}O$ and S in the Chukchi Sea vary both seasonally and spatially (Yamamoto-Kawai et al., 2008). The variation is attributable to pronounced seasonal variations in the Bering Strait freshwater (Woodgate and Aagaard, 2005) and river runoff fluxes (Holmes et al., 2012). Given that our study was carried out during the summer of 2017, the spatial distributions of freshwater components from this study should be considered a summertime snapshot of freshwater distribution in 2017.

In the western Arctic Ocean, river runoff (e.g., Siberian and North American rivers) is known to be the major source of freshwater in the surface layer (Yamamoto-Kawai et al., 2005, 2008; Pemberton et al., 2014). Previous studies (e.g., Morison et al., 2012; Bluhm et al., 2015)

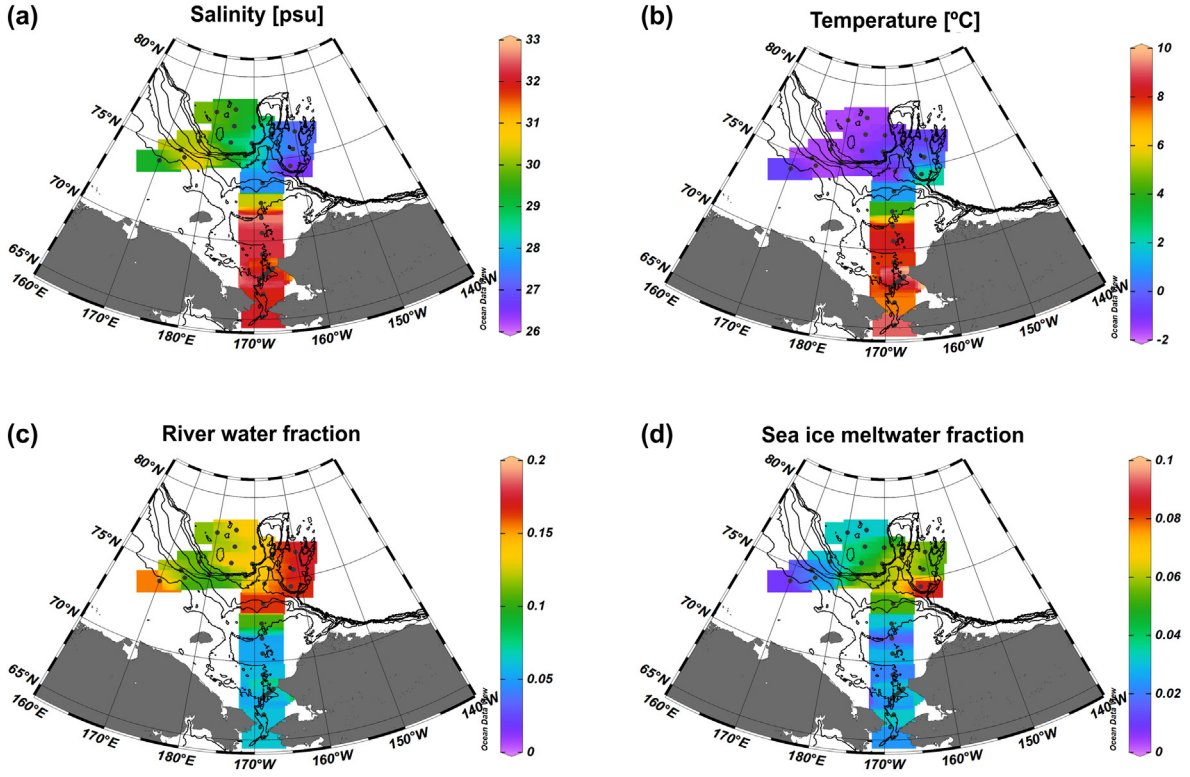

Fig. 2. Spatial distributions of (a) sea surface salinity (SSS), (b) sea surface temperature (SST), (c) river water (f_{river}), and (d) sea-ice meltwater fractions ($f_{sea\ ice\ melt}$) in the surface layer of the Chukchi Sea in the summer of 2017.

have reported that the accumulation of river water is especially pronounced in the Canada Basin, where the convergent winds of the atmospheric Beaufort High accumulate low salinity waters from both North America and Siberia within the anticyclonic Beaufort Gyre. Thus, the lowest SSS and higher freshwater fractions in the eastern stations are likely the result of the influence of the Beaufort Gyre, facilitating the long-term retention of freshwater (Hansell et al., 2004).

The observation of the higher f_{river} at the eastern stations located in near the Canada Basin does not necessarily mean that North American rivers (e.g., the Mackenzie River) are the main source of freshwater here. Using the relationship between S and alkalinity, Yamamoto-Kawai et al. (2005, 2009) reported that freshwater in the Canada Basin mainly consisted of Siberian river water and freshwater carried by Pacific water whereas proportions from the Mackenzie River were comparatively low except for the surface water at a few stations. In addition, Morison et al. (2012) reported that Pacific water and Eurasian runoff were the dominant fractions of freshwater in the upper 200 m of the Beaufort Sea, indicating the importance of Siberian river water as a freshwater source in the Pacific Arctic. Due to the limitations of the adopted method for tracing freshwater, we are unable to further consider the sources of river water in the northern Chukchi Sea; however, as the influence of Siberian rivers was found in the Canada Basin (Yamamoto-Kawai et al., 2009), f_{river} values in the northern Chukchi Sea are likely influenced by inputs from both Siberian and North American river waters.

3.2. Spatial distribution of DOC concentrations

In the southern Chukchi Sea, the DOC concentration in the surface layer ranged from 64 to 134 μM C (Fig. 3a), which was similar to that previously observed during early summer (Tanaka et al., 2016). The highest values of DOC (134 and 118 μM C) were observed near the Bering Strait (i.e., station 1) and at the station closest to the Alaskan coast (i.e., station 8), respectively. Alaska Coastal Water (ACW) is known to flow northward on the eastern side of the northern Bering and Chukchi Seas (Grebmeier et al., 2006), which contains high DOC with terrigenous characteristics from the Alaskan rivers (e.g., the Yukon River) (D'Sa et al., 2014). In addition, the southern Chukchi Sea is one of the most biologically productive regions due to the nutrients supplied by the Anadyr Water (AW) and Bering Shelf Water (BSW) (Grebmeier et al., 2006; Nishino et al., 2016). Indeed, high chlorophyll-a (Chl-a) concentrations were observed in the southern Chukchi Sea ranging from 0.11 to 10.8 mg m^{-3} (average: 3.27 ± 3.47 mg m^{-3}) (Fig. S2). Thus, the high Chl-a concentrations and the slightly higher f_{river} value at station 8 associated with the influence of the ACW (Fig. 2c) suggest the combined influence of both marine and terrestrial DOC origins in the surface waters.

In the northern Chukchi Sea, the DOC concentrations ranged from 66 to 94 μM C, with an average of 73 ± 6 μM C, which is similar to those reported for summer (Letscher et al., 2011; Tanaka et al., 2016). However, unlike the SSS, the DOC concentrations showed no clear distinction in distribution between the eastern and western stations (range: 67–79 μM C and mean: 73 ± 4 μM C versus range: 66–94 μM C and mean: 73 ± 8 μM C, respectively). Although no regional differences in bulk DOC concentrations were observed in the northern Chukchi Sea, the DOC derived from river runoff (i.e., riverine DOC) is expected to vary similarly to the case for the river water fraction.

3.3. Estimation of riverine DOC and its spatial distribution

DOC_{river} is a key factor determining riverine DOC concentrations (Eq. (4)). As described in Section 2.5.2, for the initial DOC concentration in river runoff in the southern Chukchi Sea we used a value of 350 μM C as derived from the Yukon River (Mathis et al., 2007) as the major contributor of terrigenous DOC to the Chukchi Shelf (Mathis et al., 2007; Tanaka et al., 2016). On the other hand, river water in the northern Chukchi Sea can be derived from regional sources, such as North American and East Siberian rivers as well as the Bering Strait inflow (Cooper et al., 2005). In addition, river runoff delivered to the eastern Arctic has a shelf residence time of 2–5 years before passing offshore (Letscher et al., 2011), thus resulting in ~30% of riverine DOC removal on the shelves (Cooper et al., 2005). In contrast, terrigenous DOC in river runoff to the western Arctic transits relatively narrow continental shelves, quickly passing offshore to mix with older waters that have recirculated within the Beaufort Gyre for a decade (Hansell et al., 2004; Letscher et al., 2011). This existing understanding suggests that there might be a difference in the removal rate of terrigenous DOC between the eastern and western Arctic. Observations of Siberian and North American river waters (Yamamoto-Kawai et al., 2009) imply that special caution should be taken into the determination of initial DOC concentrations in river runoff.

Plots of DOC versus S have long been used in the Arctic Ocean (e.g., Cauwet and Sidorov, 1996; Kattner et al., 1999; Hansell et al., 2004; Shin and Tanaka, 2004; Cooper et al., 2005; Mathis et al., 2005; Mathis et al., 2007; Mathis et al., 2009; Alling et al., 2010; Letscher et al., 2011) because it provides useful information regarding the removal of terrigenous DOC and its mixing between river and marine waters. For example, previous studies (e.g., Hansell et al., 2004; Alling et al., 2010; Letscher et al., 2011) derived the zero-salinity (100% river water) DOC value from the relationship between DOC and S to quantify the removal of terrigenous DOC in the Arctic Ocean. The zero-salinity DOC value obtained from the regression can also be used to infer the DOC concentration of the river water fraction, as previously applied for the

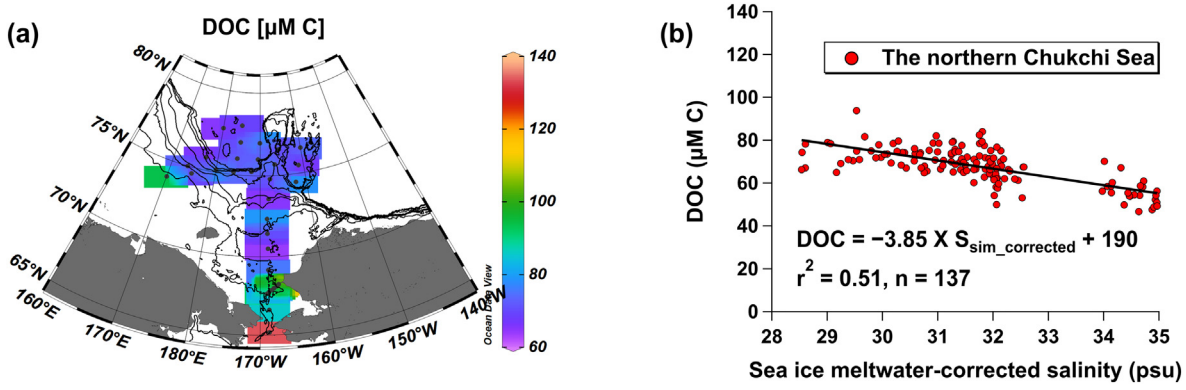

Fig. 3. Spatial distribution of (a) dissolved organic carbon (DOC) (μM C) and (b) plot of DOC (μM C) versus sea-ice meltwater-corrected salinity ($S_{sim\_corrected}$) observed in the northern Chukchi Sea in the summer of 2017.

eastern and western Arctic (Hansell et al., 2004; Cooper et al., 2005; Letscher et al., 2011). In this study, we used the relationship between DOC and S to differentiate riverine DOC from the DOC observed in the northern Chukchi Sea. However, sea-ice meltwater, especially in the northern Chukchi Sea, during the summer season may dilute the DOC concentration and S (Mathis et al., 2005). Thus, we used the following equation to calculate sea-ice meltwater-corrected S (Yamamoto-Kawai et al., 2009):

$$\text{Sea ice meltwater}-\text{corrected S} = (S - S_{\text{sea ice melt}} f_{\text{sea ice melt}})/(1 - f_{\text{sea ice melt}}) \quad (5)$$

where the calculated sea-ice meltwater-corrected S ($S_{sim\_corrected}$) indicates S in waters that have no influence from sea-ice meltwater. During the study cruise, DOC concentrations were correlated with $S_{sim\_corrected}$ in the northern Chukchi Sea (DOC (μM C) $= -3.85 \times S_{sim\_corrected}$ (psu) + 190 μM C, $r^2 = 0.51$, $p < 0.01$) (Fig. 3b). The zero-salinity intercept of 190 μM C for DOC was similar to that obtained for the northeastern Chukchi Sea (DOC (μM C) $= -3.63 \times$ salinity (psu) + 186 μM C, Mathis et al., 2009) and the Beaufort Gyre (DOC (μM C) $= -2.60 \times$ salinity (psu) + 154 μM C, Hansell et al., 2004). However, this zero-salinity intercept value (i.e., 190) was much lower than for the eastern Arctic, i.e., in the Makarov and Eurasian Basin (DOC (μM C) $= -7.60 \times$ salinity (psu) + 331 μM C, Letscher et al., 2011) in the East Siberian Sea east of 160°E, with a zero-salinity intercept of 592 (Alling et al., 2010). This suggests the substantial removal of terrigenous DOC in the western Arctic (Hansell et al., 2004) and that aged river water might be contained in the f_{river} component of in the northern Chukchi Sea, whose DOC concentrations degraded over the decade-long circulation of surface waters (Hansell et al., 2004; Letscher et al., 2011). Thus, we used a zero-salinity intercept value of 190 μM C, as being representative of the initial DOC concentration in river runoff entering the northern Chukchi Sea. This is a more reasonable approach than using the average DOC concentration in the major Arctic rivers draining into the northern Chukchi Sea, due to the degradation of terrigenous DOC during its transport.

The spatial distribution of the estimated riverine DOC in the surface layer and its contribution to the DOC are shown in Fig. 4. The riverine DOC concentration ranged from 16 to 37 μM C in the southern Chukchi Sea, from 24 to 33 μM C at the eastern stations, and from 19 to 29 μM C at the western stations of the northern Chukchi Sea, with averages of 23 ± 6, 29 ± 4, and 23 ± 3 μM C, respectively. The mean contributions of riverine DOC accounted for 27 ± 9% (range: 17–47%) of the DOC in the southern Chukchi Sea, 39 ± 6% (range: 32–49%) at the eastern stations, and 31 ± 4% (range: 25–37%) at the western stations of the northern Chukchi Sea. These results indicate that the contribution of riverine DOC is largest at the eastern stations of the northern Chukchi Sea, probably due to the pronounced accumulation of river water within the anticyclonic Beaufort Gyre and the long residence time of water in the gyre. This is supported by the lower values of the chromophoric dissolved organic matter (CDOM) absorption coefficient at 254 nm (a_{254}) observed for the eastern stations (0.15–0.25 m^{-1}) compared to the western stations (0.21–0.36 m^{-1}) of the northern Chukchi Sea (Fig. S3). This reflects the photobleaching of CDOM, which is likely enhanced in the highly stratified surface waters at the eastern stations (Logvinova et al., 2015), where the DOC contains more aged riverine DOC compared to the western stations.

The mean contribution of riverine DOC from this study is in a good agreement with a previous study conducted in the Makarov Basin, where riverine DOC contributed 25% to the total DOC (Wheeler et al., 1997), but is lower than estimates for the Laptev Sea at 60% (Kattner et al., 1999). This difference suggests that transpolar drift, as a barrier to mixing, effectively separates the eastern and western Arctic Ocean water masses (Manizza et al., 2009).

It is worth noting that there are substantial seasonal variabilities in river discharge (Holmes et al., 2012), DOC concentrations and fluxes (Holmes et al., 2012; Le Fouest et al., 2018), and the biodegradability of DOC (Holmes et al., 2008; Mann et al., 2012; Wickland et al., 2012), with higher values during the spring freshet and lower values during summer low-flow conditions, resulting in a large portion of the annual DOC export from Arctic rivers over a relatively short period (Dittmar and Kattner, 2003; Raymond et al., 2007; Cooper et al., 2008; McClelland et al., 2012). Due to the strong dependence of the microbial community on the amount and quality of DOC, the variations in DOC properties have critical effects on the microbial loop, which will, in turn, most likely affect the marine ecosystem (Mathis et al., 2005; Mathis et al., 2007; McClelland et al., 2012; Brogi et al., 2019). In this study, riverine DOC concentration was estimated during the limited sampling period (i.e., in the summer of 2017). Given the seasonal variabilities mentioned above, our results should be considered to be representative of riverine DOC in the Chukchi Sea throughout the sampling period only.

3.4. Fluorescence properties of DOM

3.4.1. Fluorescence components identified by PARAFAC modeling

Fluorophores in seawater samples can be classified into two primary components based on their peak positions (Fig. 5). The fluorescence peaks of component 1 (C1) at Ex/Em wavelengths of 230/430 nm were similar to those of terrestrial humic-like fluorophore and peak A reported in the literature (Coble, 1996; Coble et al., 1998; Stedmon et al., 2003; Ishii and Boyer, 2012). Component 2 (C2) has a primary (and secondary) fluorescence peak at an Ex/Em wavelength of 225(280)/345 nm. The spectral features of C2 were similar to tryptophan-like fluorophores, which have been regarded as phytoplankton-derived (or ice algae-derived) protein-like components in the polar ocean as well as oceanic waters (Stedmon et al., 2007, 2011b; Brogi et al., 2019). Although combinations of the two components explain the variations in FDOM in the seawater samples, here we used only C1 to trace river water because C1 is

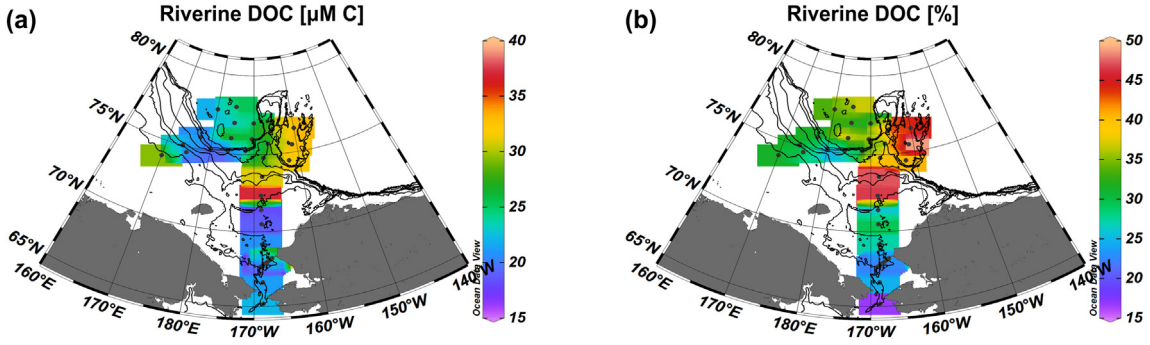

Fig. 4. Spatial distributions of (a) riverine DOC (μM C) concentration and (b) contribution of riverine DOC to the observed DOC (%) in the surface layer of the Chukchi Sea in the summer of 2017.

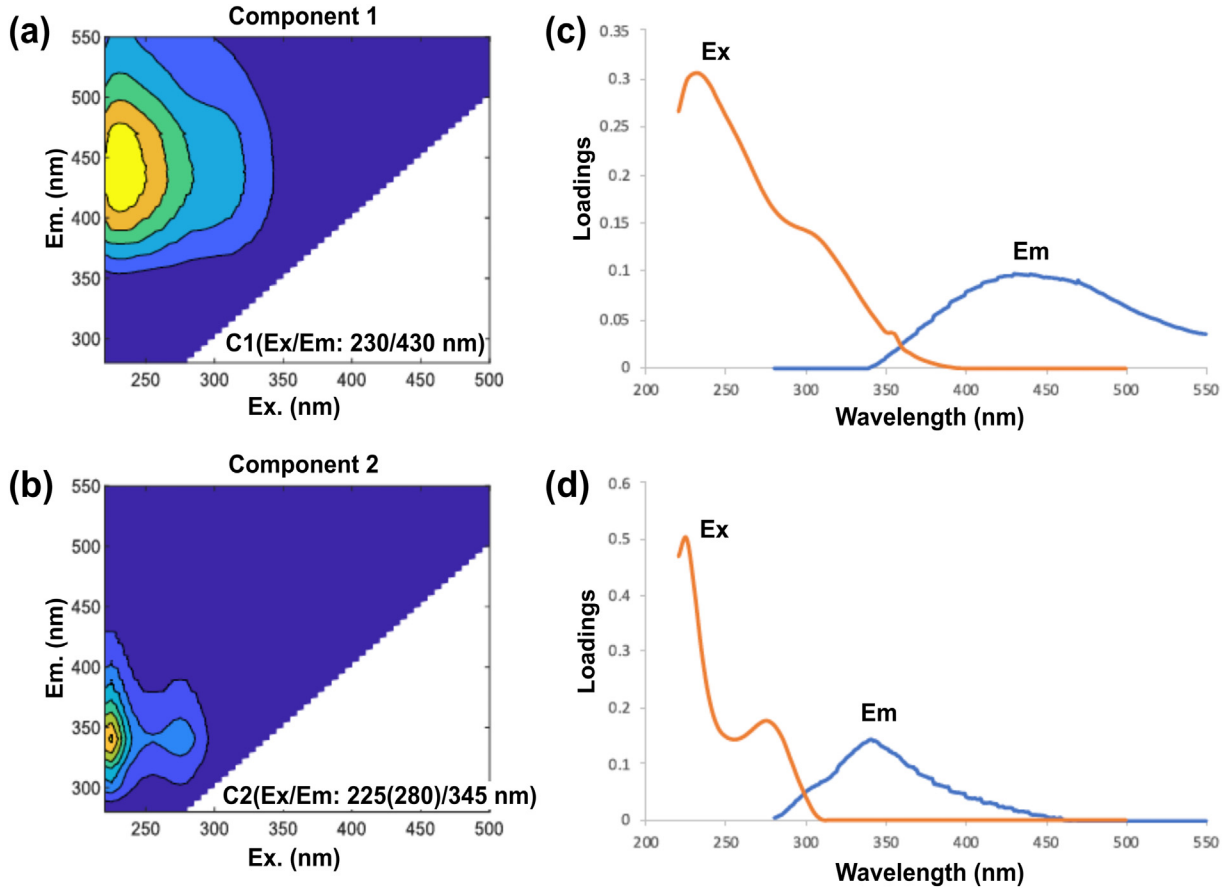

Fig. 5. EEM contour plots of fluorescent components (a) C1 and (b) C2 identified by PARAFAC in the seawater samples collected from the Chukchi Sea, with the excitation (orange line) and emission (blue line) spectra of (c) C1 and (d) C2. (For interpretation of the references to colour in this figure legend, the reader is referred to the web version of this article.)

known to be abundant in DOM dominated by terrestrial humic-like materials, such as DOM from soil extractions, forested streams, and river runoff (Ishii and Boyer, 2012; Walker et al., 2013).

3.4.2. Spatial distribution of humic-like component and its relationships with sea-ice meltwater-corrected salinity and river water fraction

In many studies, DOM fluorescence (i.e., terrestrial humic-like components) have been used as a proxy for tracing the export of terrestrial organic matter via rivers into various oceanic regions (e.g., Stedmon and Markager, 2005; Murphy et al., 2008; Guéguen et al., 2012; D'Sa et al., 2014; Goncalves-Araujo et al., 2016). This implies that the dynamics (e.g., input, mixing, and removal) of riverine DOM can be inferred from the spatial and temporal variability of the humic-like component in the studied regions. As shown in Fig. 6, the spatial variability of the humic-like C1 was similar to that of f_{river} (Fig. 2c), showing that C1 is associated with terrestrial riverine inputs. The spatial distribution of the fluorescence intensity of the humic-like C1 in the surface layer generally exhibited a clear pattern, with the lowest values occurring in the southern Chukchi Sea (range: 0.25–0.34 R.U., mean: 0.29 ± 0.031 R.U.) and higher values in the northern Chukchi Sea ranging from 0.26 to 0.52 R.U. (mean: 0.41 ± 0.06 R.U.). Meanwhile, these values were higher at the eastern stations (range: 0.34–0.52 R.U., mean: 0.44 ± 0.06 R.U.) than the western stations (range: 0.26–0.42 R.U., mean: 0.38 ± 0.05 R.U.).

The humic-like C1 from this study shows resistance to photodegradation (Stedmon and Markager, 2005; Ishii and Boyer, 2012; Yamashita et al., 2015), although C1 can be photodegraded by ultraviolet C (UVC, 290 nm or less) light because of the correspondence between its excitation peak (absorption) wavelength and the region of the light (Ishii and Boyer, 2012). However, it is notable that UVC light is sparse in terrestrial sunlight and most UVC is rapidly attenuated prior to distribution in the water column (Diffey, 2002). Furthermore, due to the specific conditions of the Arctic Ocean, including ice cover, low sun angle, and a limited daylight period (Stedmon et al., 2011a; Tanaka et al., 2016), the photodegradation of the humic-like C1 is likely limited. Thus, the highest C1 fluorescence intensity at the eastern stations suggests that humic-like C1 has photo-resistant characteristics compared to a_{254} (Fig. S3), and that more aged riverine DOM can accumulate within the Beaufort Gyre due to the long residence time.

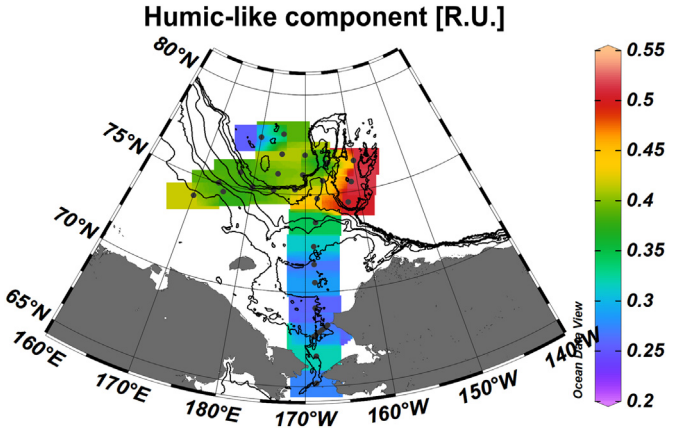

Fig. 6. Spatial distribution of the humic-like C1 (R.U.) observed in the surface layer of the Chukchi Sea in the summer of 2017.

In addition, humic-like C1 can be resistant to internal processes of degradation (i.e., it is biologically unavailable, Ishii and Boyer, 2012), revealing conservative mixing behavior as aquatic systems transition from fresh to saline conditions (e.g., Coble, 2007; Osburn and Stedmon, 2011). Based on this characteristic, we investigated the relationships between humic-like C1 and $S_{sim\_corrected}$ and f_{river} to improve understanding of riverine DOM dynamics in the study region. As expected, the humic-like fluorescence C1 intensity-$S_{sim\_corrected}$ relationship exhibited generally decreasing trends with increasing $S_{sim\_corrected}$ (Fig. 7a); however, interestingly, two negative relationships were observed over the $S_{sim\_corrected}$ range of 28 to 33 psu–one between the samples collected from the eastern and western stations of the northern Chukchi Sea (C1 (R.U.) $= -0.043 \times S_{sim\_corrected}$ (psu) $+ 1.7$ R.U., $r^2 = 0.85$) and one between the samples collected in the southern Chukchi Sea and several eastern stations of the northern Chukchi Sea (C1 (R.U.) $= -0.027 \times S_{sim\_corrected}$ (psu) $+ 1.1$ R.U., $r^2 = 0.84$). It is clear, therefore, that the humic-like C1 fluorescence intensities in the southern and northern Chukchi Sea regions are distinct with respect to $S_{sim\_corrected}$, although some of the data observed at the eastern stations appeared to be a mixture of the humic-like C1 from the southern Chukchi Sea. These results suggest that different Arctic river waters with distinct humic-like C1 characteristics are conservatively mixed in the northern Chukchi Sea (Fig. 7b). Walker et al. (2013) reported that a humic-like FDOM component (Ex/Em: 250(310)/432 nm), which is very similar to the C1 in our study, was the most predominant fluorescent component in major Arctic rivers, including the Mackenzie, Lena, Kolyma, Ob, and Yenisei Rivers. These authors also found differences in FDOM intensities between the rivers and seasons; the highest intensity was measured in the Lena River and lowest in the Mackenzie River during spring freshet due to general watershed characteristics of vegetation, topography, and hydrology. Furthermore, the ACW is primarily advected northward by the Alaskan Coastal Current (ACC), which is formed predominantly from coastal runoff along the Alaskan coast (Pisareva et al., 2015), with the freshwater transported by the ACC ultimately contributing to the reservoir of freshwater in the Beaufort Gyre (Pickart et al., 2013). Consequently, the relationships between the samples collected from the southern Chukchi Sea and the eastern stations of the northern Chukchi Sea (i.e., the black lines in Fig. 7a and b) can be explained by the entrainment of riverine DOM delivered by the ACW that enters the northern Chukchi Sea through the Bering Strait, bringing terrigenous characteristics of the Alaskan rivers to the Beaufort Gyre. On the other hand, a possible explanation for the relationships observed in the northern Chukchi Sea (i.e., the red lines in Fig. 7a and b) is the mixing of the humic-like C1 derived from the Eurasian and North American rivers—rather than the Yukon River—which have different FDOM characteristics (Walker et al., 2013) in the northern Chukchi Sea. We cannot differentiate quantify the amount of humic-like C1 derived from the Arctic river in the northern Chukchi Sea. However, the relationships we have identified with the humic-like C1 were much more significant than those with the absorption coefficient at 254 nm (or chromophoric DOM), suggesting that the C1 is a reliable tracer for riverine DOM in the Chukchi Sea (Fig. S4). Furthermore, riverine DOM derived from the southern Chukchi Sea (probably the Yukon River) is distinguishable from those of other Arctic rivers.

3.5. Vertical distribution of riverine DOM

The vertical distributions of DOC and riverine DOC concentrations at all stations are shown in Fig. 8a and b. The DOC concentrations ranged from 47 to 134 μM C, with the highest values in the surface layer. Values decreased with depth, becoming relatively constant at 51 ± 4 μM C at depths of 250–450 m (Fig. 8a), suggesting a broadly uniform background concentration of refractory DOC. In the southern Chukchi Sea, higher DOC concentrations were observed (range: 51–134 μM C, average: 80 ± 15 μM C), especially in the upper 50 m, due to the strong influence of marine DOC derived from high marine biological production, likely driven by the vertical supply of nutrients to the euphotic zone by the AW ($32.5 < S < 33$) and BSW ($31.8 < S < 32.5$) (Fig. 8f) (Grebmeier et al., 2006; Codispoti et al., 2013; Nishino et al., 2016). In comparison, the DOC concentrations at the eastern and western stations of the northern Chukchi Sea ranged from 48–84 μM C to 47–94 μM C with averages of 69 ± 9 μM C and 67 ± 9 μM C, respectively.

The distribution of terrigenous DOM in the Arctic Ocean is controlled by physical mixing, regional difference in riverine sources and the quality of the organic material related to remineralization rates, and water residence times (Manizza et al., 2009; Stedmon et al., 2011a). In our study region, the riverine DOC concentrations ranged from 0.18 to 40 μM C (average: 19 ± 8 μM C) with a general decreasing trend from the surface to the bottom layers (Fig. 8b). In the southern Chukchi Sea, the riverine DOC concentrations varied from 15 to 40 μM C with an average of 22 ± 6 μM C, contributing 28 ± 10% to the DOC concentrations. In comparison, the riverine DOC concentrations in the northern Chukchi Sea ranged from 0.18 to 33 μM C with an average of 18 ± 8 μM C, which accounted for 25 ± 11% of the observed DOC. The riverine DOC

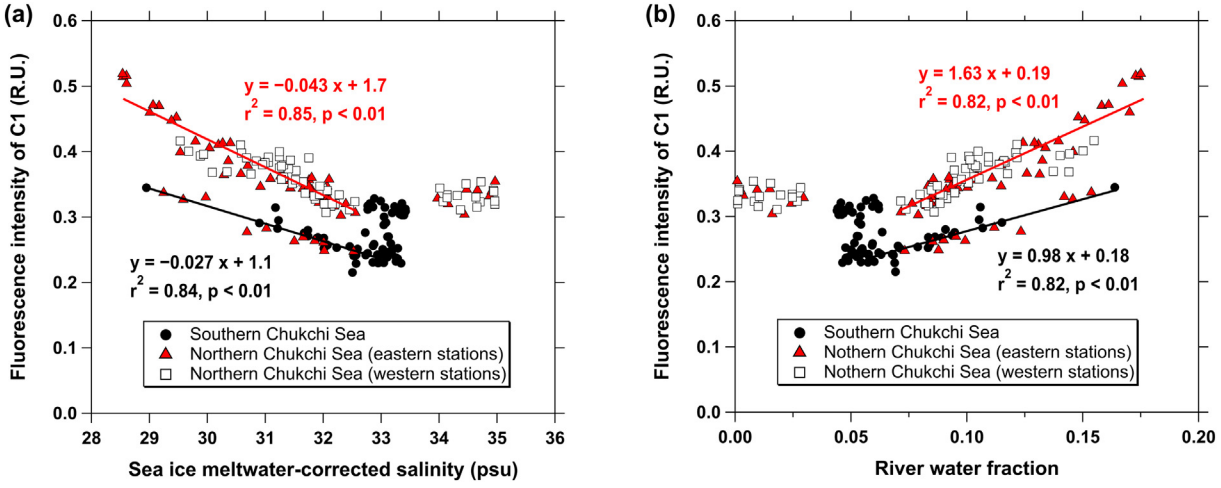

Fig. 7. Fluorescence intensity of humic-like C1 (R.U.) versus property plots for (a) sea-ice meltwater-corrected salinity ($S_{sim\_corrected}$) and (b) the river water fraction (f_{river}) observed in the southern Chukchi Sea (black circle), and the eastern (red triangle) and western stations (white square) of the northern Chukchi Sea in the summer of 2017. Red lines in (a) and (b) indicate the relationships between the fluorescence intensity of humic-like C1 and $S_{sim\_corrected}$ and f_{river} of samples collected at the eastern and western stations of northern Chukchi Sea, respectively. The relationships of fluorescence intensity of humic-like C1 with $S_{sim\_corrected}$ and f_{river} observed between the samples collected in the southern Chukchi Sea, and the eastern stations of the northern Chukchi Sea (black lines), are also shown in (a) and (b), respectively. (For interpretation of the references to colour in this figure legend, the reader is referred to the web version of this article.)

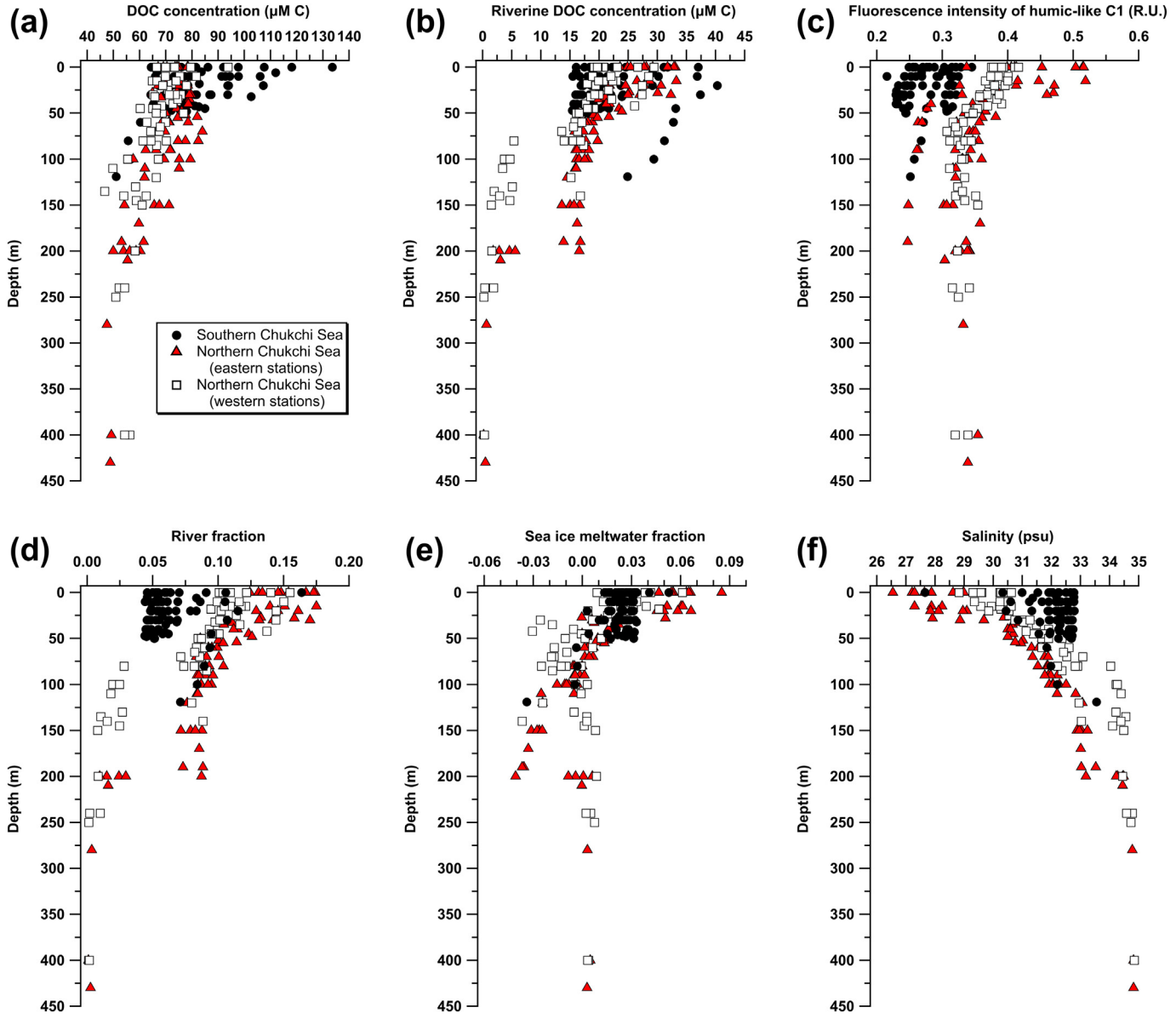

Fig. 8. Vertical profiles of (a) dissolved organic carbon (DOC) (μM C), (b) riverine DOC (μM C), (c) fluorescence intensity of humic-like C1 (R.U.), (d) the river water fraction (f_{river}), (e) the sea-ice meltwater fractions ($f_{sea\ ice\ melt}$), and (f) salinity (S) (psu) observed in the southern Chukchi Sea (black circle), and the eastern (red triangle) and western stations (white square) of northern Chukchi Sea in the summer of 2017. (For interpretation of the references to colour in this figure legend, the reader is referred to the web version of this article.)

concentrations at the eastern stations (range: 0.18–33 μM C, average: 19 ± 8 μM C) were comparable to those of the western stations (range: 0.20–29 μM C, average: 15 ± 8 μM C) of the northern Chukchi Sea, accounting for 27 ± 11% and 22 ± 11% of the observed DOC, respectively. Overall, the contributions of riverine DOC were less than 30%, suggesting that most of the observed DOC is of marine origin. The estimated riverine DOC concentrations in the northern Chukchi Sea were somewhat lower than those in the southern Chukchi Sea, although relatively high values and contributions were observed in the surface layer of the northern Chukchi Sea (Fig. 4). These results suggest that the water in the southern Chukchi Sea is vertically well mixed compared to the northern Chukchi Sea (Fig. 8f), and that more aged riverine DOC is contained in the northern Chukchi Sea (Hansell et al., 2004; Letscher et al., 2011). In addition, despite the strong influence of river water in the upper 50 m (Fig. 8b and d), riverine DOC and f_{river} were found in the upper halocline layer (32 psu < S < 33.5 psu, at depths between 50 and 200 m) (Fig. 8f) (Codispoti et al., 2005; Alkire et al., 2019), suggesting the entrainment of river water and riverine DOC.

The vertical distribution of humic-like C1 exhibited clear differences in fluorescence intensity between the southern and northern Chukchi Sea, with higher values in the northern Chukchi Sea (Fig. 8c). This can be attributed to the distinct humic-like C1 characteristics among different Arctic river waters (Walker et al., 2013). Furthermore, it was observed that riverine DOM delivered by the ACW (with lower humic-like C1 intensity from Alaskan rivers) was entrained into the Beaufort Gyre in the northern Chukchi Sea (see Section 3.4.2). Overall, the humic-like C1 fluorescence intensities at the eastern stations were higher than those at the western stations because of the accumulation of riverine DOM within the anticyclonic Beaufort Gyre.

In the northern Chukchi Sea, except for some stations, the humic-like C1 fluorescence intensities decreased with increasing depth, reaching relatively constant values of 0.35 ± 0.06 R.U. in the lower halocline layer (S > 34 psu, depths between 250 and 450 m) where saline Atlantic Water dominates (Fig. 8f) (Codispoti et al., 2005; Alkire et al., 2019). Similar results were observed in the Eurasian and Canada basins by Stedmon et al. (2011a), who reported that the CDOM signal in both

the polar mixed layer (0–50 m) and the Atlantic halocline layer originating from the Fram Strait and Barents Sea were similar to the CDOM supplied by the major Arctic rivers. This indicates that the Arctic rivers are the dominant sources of CDOM and that riverine CDOM is entrained into the halocline layer.

Although riverine DOM (i.e., riverine DOC and humic-like C1) and f_{river} were predominantly distributed in the upper 50 m of the water column, their vertical profiles suggest that river runoff-enriched water is exported from the surface to the halocline layer, as discussed in the following section.

3.6. Influence of sea-ice formation on the vertical distribution of riverine DOM

As shown in Fig. 8b—d, pronounced riverine DOC and f_{river} values were found in the upper halocline layer, where $f_{sea\ ice\ melt}$ dropped below zero (Fig. 8e) indicating the occurrence of brine rejection from growing sea ice (Yamamoto-Kawai et al., 2005). Sea-ice formation at the surface during winter leads to brine formation (negative $f_{sea\ ice\ melt}$) (Yamamoto-Kawai et al., 2005; Goncalves-Araujo et al., 2016). Thus, the release and sinking of dense brines from sea ice could be an important transport pathway for DOM and other chemical species (e.g., nutrients) to the halocline layer (Aagaard et al., 1985; Giannelli et al., 2001; Thomas et al., 2001; Macdonald et al., 2002; Amon, 2004; Guéguen et al., 2007). Moreover, DOM is rejected from sea ice during its formation (Amon, 2004). Thus, the riverine DOM and f_{river} observed in the upper halocline layer in this study clearly demonstrate that river runoff-enriched water is delivered from the surface to the upper halocline layer by rejected brine from sea ice during winter. As such, sea-ice formation is a key in the transport of riverine DOM to the upper halocline layer in the northern Chukchi Sea. The riverine DOM delivered into the halocline layer is eventually exported to the central Arctic Ocean and, subsequently, to the North Atlantic (Hansell et al., 2004; Guéguen et al., 2007; Stedmon et al., 2011a). These results suggest that the rapid retreat and thinning of sea ice in the Arctic Ocean (Cavalieri and Parkinson, 2012) could alter the global carbon cycle as well as ocean circulation.

4. Conclusions

River runoff was the main source of freshwater in the surface layer of the northern Chukchi Sea. In particular, higher values of f_{river} and riverine DOC concentrations were observed in the surface layer of the eastern stations. In addition, the highest contribution of riverine DOC was found in the eastern stations, accounting for 39 ± 6% (range: 32–49%) of the total DOC concentration. These results suggest that older river water and riverine DOC accumulate within the Beaufort Gyre due to a long residence time, which is supported by higher humic-like fluorescence C1 intensities in the region.

The humic-like C1 fluorescence intensities in the southern and northern Chukchi Sea regions were distinct; the relationships between the humic-like fluorescence intensity and $S_{sim\_corrected}$ and f_{river} revealed that different Arctic river waters (with these distinct humic-like C1 characteristics) are mixed in the northern Chukchi Sea. This shows that DOM fluorescence is a powerful tracer of river water and riverine DOM in our study region. The vertical distributions of riverine DOC, humic-like C1 intensity, f_{river}, and $f_{sea\ ice\ melt}$ indicated that river runoff-enriched water is delivered from the surface to the upper halocline layer by deep convective mixing due to brine rejection during sea-ice formation (negative $f_{sea\ ice\ melt}$). This process is a key mechanism throughout which riverine DOM is transferred to the upper halocline layer in the northern Chukchi Sea.

It is worth noting that the spatial distributions of freshwater components, riverine DOC, and the humic-like component in the Chukchi Sea were investigated during the limited sampling period, which should be considered to be representative of those throughout the sampling period only. Nevertheless, the results from this study could be valuable for filling the data gap, especially for the northwestern Chukchi Sea during summer, and could also be helpful for the validation of the modeling of riverine DOC dynamics.

Recent warming temperatures (Overland et al., 2019) and consequent permafrost thaw (Romanovsky et al., 2010) and increases in riverine discharge (Holmes et al., 2018) in the Arctic Ocean will induce alterations in the quantity and distribution of terrigenous DOM with dramatic consequences for Arctic biogeochemical cycles. This will ultimately alter the air-to-sea flux of atmospheric CO_2 and carbon export (Letscher et al., 2011). In addition, the reduction in multi-year ice extent (Comiso, 2012; Perovich et al., 2020) will likely increase carbon export to the ocean's deep layers. Hence, further studies including the long-term monitoring of variations in riverine DOM are required to better understand how the Arctic Ocean will respond to increasing river water and riverine DOM inputs.

CRediT authorship contribution statement

Jinyoung Jung: Conceptualization, Methodology, Investigation, Writing – original draft, Writing – review & editing. **Jin Eui Son:** Investigation, Writing – original draft, Writing – review & editing. **Yun Kyung Lee:** Formal analysis. **Kyoung-Ho Cho:** Investigation, Writing – review & editing. **Youngju Lee:** Investigation, Writing – review & editing. **Eun Jin Yang:** Investigation, Writing – review & editing. **Sung-Ho Kang:** Writing – review & editing, Project administration, Funding acquisition. **Jin Hur:** Supervision, Writing – review & editing, Resources.

Declaration of competing interest

The authors declare that they have no known competing financial interests or personal relationships that could have appeared to influence the work reported in this paper.

Acknowledgements

This research is a part of the project titled “Korea-Arctic Ocean Observing System (K-AOOS)”, the Korea Polar Research Institute (KOPRI) 2016245, funded by the Ministry of Oceans and Fisheries (MOF), Korea. It is also supported by a grant from the National Research Foundation of Korea (NRF) funded by the Korean government (2020R1A4A2002823).We are grateful to the captain and crew of the IBR/V Araon for their enthusiastic assistance during the ARA08B cruise.

Appendix A. Supplementary data

Supplementary data to this article can be found online at https://doi.org/10.1016/j.scitotenv.2021.145542.

References

Aagaard, K., Swift, J.H., Carmack, E.C., 1985. Thermohaline circulation in the Arctic Mediterranean Seas. J. Geophys. Res. 90, 4833–4846. https://doi.org/10.1029/JC090iC03p04833.

Abbott, B.W., Larouche, J.R., Jones, J.B., Bowden, W.B., Balser, A.W., 2014. Elevated dissolved organic carbon biodegradability from thawing and collapsing permafrost. J. Geophys. Res. 119, 2049–2063. https://doi.org/10.1002/2014JG002678.

Alkire, M.B., Rember, R., Polyakov, I., 2019. Discrepancy in the identification of the Atlantic/Pacific Front in the Central Arctic Ocean: NO versus nutrient relationships. Geophys. Res. Lett. 46, 3843–3852. https://doi.org/10.1029/2018GL081837.

Alling, V., Sanchez-Garcia, L., Porcelli, D., Pugach, S., Vonk, J.E., van Dongen, B., Mörth, C.-M., Anderson, L.G., Sokolov, A., Andersson, P., Humborg, C., Semiletov, I., Gustafsson, Ö., 2010. Nonconservative behavior of dissolved organic carbon across the Laptev and East Siberian seas. Glob. Biogeochem. Cycles 24, GB4033. https://doi.org/10.1029/2010GB003834.

Amon, R.M.W., 2004. The role of dissolved organic matter for the organic carbon cycle in the Arctic Ocean. In: Stein, R., Macdonald, R.W. (Eds.), The Organic Carbon Cycle in the Arctic Ocean. Springer, Berlin, pp. 83–99.

Bates, N.R., Mathis, J.T., 2009. The Arctic Ocean marine carbon cycle: evaluation of air-sea CO_2 exchanges, ocean acidification impacts and potential feedbacks. Biogeosciences 6, 2433–2459. https://doi.org/10.5194/bg-6-2433-2009.

Bauch, D., 1995. The distribution of $\delta^{18}O$ in the Arctic Ocean: implications for the freshwater balance of the halocline and the sources of deep and bottom waters. Reports on Polar Research. vol. 159. AWI, Bremerhaven, Germany, pp. 1–144.
Bluhm, B.A., Kosobokova, K.N., Carmack, E.C., 2015. A tale of two basins: an integrated physical and biological perspective of the deep Arctic Ocean. Prog. Oceanogr. 139, 89–121. https://doi.org/10.1016/j.pocean.2015.07.011.
Brogi, S.R., Jung, J.Y., Ha, S.-Y., Hur, J., 2019. Seasonal differences in dissolved organic matter properties and sources in an Arctic fjord: implications for future conditions. Sci. Total Environ. 694, 1–9. https://doi.org/10.1016/j.scitotenv.2019.133740.
Cauwet, G., Sidorov, I., 1996. The biogeochemistry of Lena River: organic carbon and nutrients distribution. Mar. Chem. 53, 211–227.
Cavalieri, D.J., Parkinson, C.L., 2012. Arctic sea ice variability and trends, 1979–2010. Cryosphere 6, 881–889. https://doi.org/10.5194/tc-6-881-2012.
Chen, M., Price, R.M., Yamashita, Y., Jaffé, R., 2010. Comparative study of dissolved organic matter from groundwater and surface water in the Florida coastal Everglades using multi-dimensional spectrofluorometry combined with multivariate statistics. Appl. Geochem. 25, 872–880.
Chen, M., Nam, S.-I., Kim, J.-H., Kwon, Y.-J., Hong, S., Jung, J., Shin, K.-H., Hur, J., 2017. High abundance of protein-like fluorescence in the Amerasian Basin of Arctic Ocean: potential implication of a fall phytoplankton bloom. Sci. Total Environ. 599–600, 355–363. https://doi.org/10.1016/j.scitotenv.2017.04.233.
Chen, M., Jung, J., Lee, Y.K., Hur, J., 2018. Surface accumulation of low molecular weight dissolved organic matter in surface waters and horizontal off-shelf spreading of nutrients and humic-like fluorescence in the Chukchi Sea of the Arctic Ocean. Sci. Total Environ. 639, 624–632.
Coble, P.G., 1996. Characterization of marine and terrestrial DOM in seawater using excitation-emission matrix spectroscopy. Mar. Chem. 51, 325–346. https://doi.org/10.1016/0304-4203(95)00062-3.
Coble, P.G., 2007. Marine optical biogeochemistry: the chemistry of ocean color. Chem. Rev. 107, 402–418. https://doi.org/10.1021/cr050350+.
Coble, P., Del Castillo, C.E., Avril, B., 1998. Distribution and optical properties of CDOM in the Arabian Sea during the 1995 Southwest Monsoon. Deep-Sea Res. Part II 45, 2195–2223. https://doi.org/10.1016/S0967-0645(98)00068-X.
Codispoti, L.A., Flagg, C., Kelly, V., Swift, J.H., 2005. Hydrographic conditions during the 2002 SBI process experiments. Deep-Sea Res. II Top. Stud. Oceanogr. 52, 3199–3226. https://doi.org/10.1016/j.dsr2.2005.10.007.
Codispoti, L.A., Kelly, V., Thessen, A., Matrai, P., Suttles, S., Hill, V., Steele, M., Light, B., 2013. Synthesis of primary production in the Arctic Ocean: III. Nitrate and phosphate based estimates of net community production. Prog. Oceanogr. 110, 126–150. https://doi.org/10.1016/j.pocean.2012.11.006.
Comiso, J.C., 2012. Large decadal decline of the Arctic multiyear ice cover. J. Clim. 25, 1176–1193. https://doi.org/10.1175/JCLI-D-11-00113.1.
Cooper, L.W., Benner, R., McClelland, J.W., Peterson, B.J., Holmes, R.M., Raymond, P.A., Hansell, D.A., Grebmeier, J.M., Codispoti, L.A., 2005. Linkages among runoff, dissolved organic carbon, and the stable oxygen isotope composition of seawater and other water mass indicators in the Arctic Ocean. J. Geophys. Res. 110, G02013. https://doi.org/10.1029/2005JG000031.
Cooper, L.W., McClelland, J.W., Holmes, R.M., Raymond, P.A., Gibson, J.J., Guay, C.K., Peterson, B.J., 2008. Flow-weighted values of runoff tracers ($\delta^{18}O$, DOC, Ba, alkalinity) from the six largest Arctic rivers. Geophys. Res. Lett. 35, L18606. https://doi.org/10.1029/2008GL035007.
Diffey, B.L., 2002. Sources and measurement of ultraviolet radiation. Methods 28, 4–13. https://doi.org/10.1016/S1046-2023(02)00204-9.
Dittmar, T., Kattner, G., 2003. The biogeochemistry of the river and shelf ecosystem of the Arctic Ocean: a review. Mar. Chem. 83, 103–120. https://doi.org/10.1016/S0304-4203(03)00105-1.
Drozdova, A.N., Patsaeva, S.V., Khundzhua, D.A., 2017. Fluorescence of dissolved organic matter as a marker for distribution of desalinated waters in the Kara Sea and bays of Novaya Zemlya archipelago. Oceanology 57, 41–47. https://doi.org/10.1134/S0001437017010039.
Drozdova, A.N., Kravchishina, M.D., Khundzhua, D.A., Freidkin, M.P., Patsaeva, S.V., 2018. Fluorescence quantum yield of CDOM in coastal zones of the Arctic seas. Int. J. Remote Sens. 39, 9356–9379. https://doi.org/10.1080/01431161.2018.1506187.
D'Sa, E.J., Goes, J.I., Gomes, H., Mouw, C., 2014. Absorption and fluorescence properties of chromophoric dissolved organic matter of the eastern Bering Sea in the summer with special reference to the influence of a cold pool. Biogeosciences 11, 3225–3244. https://doi.org/10.5194/bg-11-3225-2014.
Eicken, H., Krouse, H.R., Kadko, D., Perovich, D.K., 2002. Tracer studies of pathways and rates of meltwater transport through Arctic summer sea ice. J. Geophys. Res. 107, 8046. https://doi.org/10.1029/2000JC000583.
Eicken, H., Gradinger, R., Gaylord, A., Mahoney, A., Rigor, I., Melling, H., 2005. Sediment transport by sea ice in the Chukchi and Beaufort Seas: increasing importance due to changing ice conditions? Deep-Sea Res. II Top. Stud. Oceanogr. 52, 3281–3302. https://doi.org/10.1016/j.dsr2.2005.10.006.
Ekwurzel, B., Schlosser, P., Mortlock, R.A., Fairbanks, R.G., 2007. River runoff, sea ice meltwater, and Pacific water distribution and mean residence times in the Arctic Ocean. J. Geophys. Res. 106, 9075–9092.
Frey, K.E., McClelland, J.W., 2009. Impacts of permafrost degradation on arctic river biogeochemistry. Hydrol. Process. 23, 169–182. https://doi.org/10.1002/hyp.7196.
Gao, T., Kang, S., Chen, R., Zhang, T., Zhang, T., Han, C., Tripathee, L., Sillanpää, M., Zhang, Y., 2019. Riverine dissolved organic carbon and its optical properties in a permafrost region of the Upper Heihe River basin in the Northern Tibetan Plateau. Sci. Total Environ. 686, 370–381. https://doi.org/10.1016/j.scitotenv.2019.05.478.
Giannelli, V., Thomas, D.N., Haas, C., Kattner, G., Kennedy, H., Dieckmann, G.S., 2001. Behaviour of dissolved organic matter and inorganic nutrients during experimental sea-ice formation. Ann. Glaciol. 33, 317–321. https://doi.org/10.3189/172756401781818572.
Goncalves-Araujo, R., Granskog, M.A., Bracher, A., Azetsu-Scott, K., Dodd, P.A., Stedmon, C.A., 2016. Using fluorescent dissolved organic matter to trace and distinguish the origin of Arctic surface waters. Sci. Rep. 6, 1–12. https://doi.org/10.1038/srep33978.
Grebmeier, J.M., Cooper, L.W., Feder, H.M., Sirenko, B.I., 2006. Ecosystem dynamics of the Pacific-influenced Northern Bering and Chukchi Seas in the Amerasian Arctic. Prog. Oceanogr. 71, 331–361. https://doi.org/10.1016/j.pocean.2006.10.001.
Guéguen, C., Guo, L., Kawai, M.Y., Tanaka, N., 2007. Colored dissolved organic matter dynamics across the shelf-basin interface in the western Arctic Ocean. J. Geophys. Res. Oceans 112, C05038. https://doi.org/10.1029/2006JC003584.
Guéguen, C., McLaughlin, F.A., Carmack, E.C., Itoh, M., Narita, H., Nishino, S., 2012. The nature of colored dissolved organic matter in the southern Canada Basin and East Siberian Sea. Deep-Sea Res. II Top. Stud. Oceanogr. 81–84, 102–113. https://doi.org/10.1016/j.dsr2.2011.05.004.
Hansell, D.A., Kadko, D., Bates, N.R., 2004. Degradation of terrigenous dissolved organic carbon in the western Arctic Ocean. Science 304, 858–861. https://doi.org/10.1126/science.1096175.
Holmes, R.M., McClelland, J.W., Raymond, P.A., Frazer, B.B., Peterson, B.J., Stieglitz, M., 2008. Lability of DOC transported by Alaskan rivers to the Arctic Ocean. Geophys. Res. Lett. 35, L03402. https://doi.org/10.1029/2007GL032837.
Holmes, R.M., McClelland, J.W., Peterson, B.J., Tank, S.E., Bulygina, E., Eglinton, T.I., Gordeev, V.V., Gurtovaya, T.Y., Raymond, P.A., Repeta, D.J., Staples, R., Striegl, R.G., Zhulidov, A.V., Zimov, S.A., 2012. Seasonal and annual fluxes of nutrients and organic matter from large rivers to the Arctic Ocean and surrounding seas. Estuar. Coasts 35, 369–382. https://doi.org/10.1007/s12237-011-9386-6.
Holmes, R.M., Shiklomanov, A.I., Suslova, A., Tretiakov, M., McClelland, J.W., Spencer, R.G.M., Tank, S.E., 2018. River discharge. Arctic Report Card: Update 2018 - Effects of Persistent Arctic Warming Continue to Mount. Arctic Research Program in the National Oceanic and Atmospheric Administration, U.S. Department of Commerce, Washington.
Ishii, S.K.L., Boyer, T.H., 2012. Behavior of reoccurring PARAFAC components in fluorescent dissolved organic matter in natural and engineered systems: a critical review. Environ. Sci. Technol. 46, 2006–2017. https://doi.org/10.1021/es2043504.
Jørgensen, L., Stedmon, C.A., Kaartokallio, H., Middelboe, M., Thomas, D.N., 2015. Changes in the composition and bioavailability of dissolved organic matter during sea ice formation. Limnol. Oceanogr. 60, 817–830. https://doi.org/10.1002/lno.10058.
Kattner, G., Lobbes, J.M., Fitznar, H.P., Engbrodt, R., Nöthig, E.-M., Lara, R.J., 1999. Tracing dissolved organic substances and nutrients from the Lena River through Laptev Sea (Arctic). Mar. Chem. 65, 25–39.
Kwok, R., Cunningham, G.F., Wensnahan, M., Rigor, I., Zwally, H.J., Yi, D., 2009. Thinning and volume loss of the Arctic Ocean sea ice cover: 2003–2008. J. Geophys. Res. Oceans 114, L01703. https://doi.org/10.1029/2009JC005312.
Lawaetz, A.J., Stedmon, C.A., 2009. Fluorescence intensity calibration using the Raman scatter peak of water. Appl. Spectrosc. 63, 936–940.
Le Fouest, V., Matsuoka, A., Manizza, M., Shernetsky, M., Tremblay, B., Babin, M., 2018. Towards an assessment of riverine dissolved organic carbon in surface waters of the western Arctic Ocean based on remote sensing and biogeochemical modeling. Biogeosciences 15, 1335–1346. https://doi.org/10.5194/bg-15-1335-2018.
Letscher, R.T., Hansell, D.A., Kadko, D., 2011. Rapid removal of terrigenous dissolved organic carbon over the Eurasian shelves of the Arctic Ocean. Mar. Chem. 123, 78–87. https://doi.org/10.1016/j.marchem.2010.10.002.
Lobbes, J.M., Fitznar, H.P., Kattner, G., 2000. Biogeochemical characteristics of dissolved and particulate organic matter in Russian rivers entering the Arctic Ocean. Geochim. Cosmochim. Acta 64, 2973–2983. https://doi.org/10.1016/S0016-7037(00)00409-9.
Logvinova, C.L., Frey, K.E., Mann, P.J., Stubbins, A., Spencer, R.G.M., 2015. Assessing the potential impacts of declining Arctic sea ice cover on the photochemical degradation of dissolved organic matter in the Chukchi and Beaufort Seas. J. Geophys. Res. Biogeosci. 120, 2326–2344. https://doi.org/10.1002/2015JG003052.
Logvinova, C.L., Frey, K.E., Cooper, L.W., 2016. The potential role of sea ice melt in the distribution of chromophoric dissolved organic matter in the Chukchi and Beaufort Seas. Deep-Sea Res. II Top. Stud. Oceanogr. 130, 28–42. https://doi.org/10.1016/j.dsr2.2016.04.017.
Macdonald, R.W., Carmack, E.C., McLaughlin, F.A., Falkner, K.K., Swift, J.H., 1999. Connections among ice, runoff and atmospheric forcing in the Beaufort Gyre. Geophys. Res. Lett. 26, 2223–2226. https://doi.org/10.1029/1999GL900508.
Macdonald, R.W., McLaughlin, F.A., Carmack, E.C., 2002. Fresh water and its sources during the SHEBA drift in the Canada Basin of the Arctic Ocean. Deep-Sea Res. Part I 49, 1769–1785. https://doi.org/10.1016/S0967-0637(02)00097-3.
Manizza, M., Follows, M.J., Dutkiewicz, S., McClelland, J.W., Menemenlis, D., Hill, C.N., Townsend-Small, A., Peterson, B.J., 2009. Modeling transport and fate of riverine dissolved organic carbon in the Arctic Ocean. Glob. Biogeochem. Cycles 23, GB4006. https://doi.org/10.1029/2008GB003396.
Mann, P.J., Davydova, A., Zimov, N., Spencer, R.G.M., Davydov, S., Bulygina, E., Zimov, S., Holmes, R.M., 2012. Controls on the composition and lability of dissolved organic matter in Siberia's Kolyma River basin. J. Geophys. Res. 117, G01028. https://doi.org/10.1029/2011JG001798.
Mann, P.J., Spencer, R.G.M., Hernes, P.J., Six, J., Aiken, G.R., Tank, S.E., McClelland, J.W., Butler, K.D., Dyda, R.Y., Holmes, R.M., 2016. Pan-Arctic trends in terrestrial dissolved organic matter from optical measurements. Front. Earth Sci. 4, 1–18. https://doi.org/10.3389/feart.2016.00025.
Mathis, J.T., Hansell, D.A., Bates, N.R., 2005. Strong hydrographic controls on spatial and seasonal variability of dissolved organic carbon in the Chukchi Sea. Deep-Sea Res. II Top. Stud. Oceanogr. 52, 3245–3258. https://doi.org/10.1016/j.dsr2.2005.10.002.
Mathis, J.T., Hansell, D.A., Kadko, D., Bates, N.R., Cooper, L.W., 2007. Determining net dissolved organic carbon production in the hydrographically complex western Arctic Ocean. Limnol. Oceanogr. 52, 1789–1799.

Mathis, J.T., Bates, N.R., Hansell, D.A., Babila, T., 2009. Net community production in the northeastern Chukchi Sea. Deep-Sea Res. II Top. Stud. Oceanogr. 56, 1213–1222. https://doi.org/10.1016/j.dsr2.2008.10.017.
McClelland, J.W., Holmes, R.M., Dunton, K.H., Macdonald, R.W., 2012. The Arctic Ocean estuary. Estuar. Coasts 35, 353–368. https://doi.org/10.1007/s12237-010-9357-3.
McGuire, A.D., Anderson, L.G., Christensen, T.R., Dallimore, S., Guo, L., Hayes, D.J., Heimann, M., Lorenson, T.D., Macdonald, R.W., Roulet, N., 2009. Sensitivity of the carbon cycle in the Arctic to climate change. Ecol. Monogr. 79, 523–555. https://doi.org/10.1890/08-2025.1.
McKnight, D.M., Boyer, E.W., Westerhoff, P.K., Doran, P.T., Kulbe, T., Andersen, D.T., 2001. Spectrofluorometric characterization of dissolved organic matter for indication of precursor organic material and aromaticity. Limnol. Oceanogr. 46, 38–48.
Morison, J., Kwok, R., Peralta-Ferriz, C., Alkire, M., Rigor, I., Andersen, R., Steele, M., 2012. Changing Arctic Ocean freshwater pathways. Nature 481, 66–70. https://doi.org/10.1038/nature10705.
Murphy, K.R., Stedmon, C.A., Waite, T.D., Ruiz, G.M., 2008. Distinguishing between terrestrial and autochthonous organic matter sources in marine environments using fluorescence spectroscopy. Mar. Chem. 108, 40–58. https://doi.org/10.1016/j.marchem.2007.10.003.
Nishino, S., Kikuchi, T., Fujiwara, A., Hirawake, T., Aoyama, M., 2016. Water mass characteristics and their temporal changes in a biological hotspot in the southern Chukchi Sea. Biogeosciences 13, 2563–2578. https://doi.org/10.5194/bg-13-2563-2016.
Osburn, C.L., Stedmon, C.A., 2011. Linking the chemical and optical properties of dissolved organic matter in the Baltic–North Sea transition zone to differentiate three allochthonous inputs. Mar. Chem. 126, 281–294. https://doi.org/10.1016/j.marchem.2011.06.007.
Overland, J.E., Hanna, E., Hanssen-Bauer, I., Kim, S.-J., Walsh, J.E., Wang, M., Bhatt, U.S., Thoman, R.L., Ballinger, T.J., 2019. Surface air temperature. Arctic Report Card: Update 2019 - Arctic Ecosystems and Communities Are Increasingly at Risk Due to Continued Warming and Declining Sea Ice. Arctic Research Program in the National Oceanic and Atmospheric Administration, U.S. Department of Commerce, Washington.
Pemberton, P., Nilsson, J., Meier, H.E.M., 2014. Arctic Ocean freshwater composition, pathways and transformations from a passive tracer simulation. Tellus Ser. A 66, 23988. https://doi.org/10.3402/tellusa.v66.23988.
Perovich, D., Meier, W., Tschudi, M., Hendricks, S., Petty, A.A., Divine, D., Farrell, S., Gerland, S., Haas, C., Kaleschke, L., Pavlova, O., Ricker, R., Tian-Kunze, X., Webster, M., Wood, K., 2020. Sea ice. Arctic Report Card: Update 2020 – The Sustained Transformation to a Warmer, Less Frozen and Biologically Changed Arctic Remains Clear. Arctic Research Program in the National Oceanic and Atmospheric Administration, U.S. Department of Commerce, Washington.
Peterson, B.J., Holmes, R.M., McClelland, J.W., Vörösmarty, C.J., Lammers, R.B., Shiklomanov, A.I., Shiklomanov, I.A., Rahmstorf, S., 2002. Increasing river discharge to the Arctic Ocean. Science 298, 2171–2173. https://doi.org/10.1126/science.1077445.
Pfirman, S., Haxby, W., Eicken, H., Jeffries, M., Bauch, D., 2004. Drifting Arctic sea ice archives changes in ocean surface conditions. Geophys. Res. Lett. 31, L19401. https://doi.org/10.1029/2004GL020666.
Pickart, R.S., Schulze, L.M., Moore, G.W.K., Charette, M.A., Arrigo, K., van Dijken, G., Danielson, S.L., 2013. Long-term trends of upwelling and impacts on primary productivity in the Alaskan Beaufort Sea. Deep-Sea Res. I Oceanogr. Res. Pap. 79, 106–121. https://doi.org/10.1016/j.dsr.2013.05.003.
Pisareva, M.N., Pickart, R.S., Spall, M.A., Nobre, C., Torres, D.J., Moore, G.W.K., Whitledge, T.E., 2015. Flow of pacific water in the western Chukchi Sea: results from the 2009 RUSALCA expedition. Deep-Sea Res. I Oceanogr. Res. Pap. 105, 53–73. https://doi.org/10.1016/j.dsr.2015.08.011.
Raymond, P.A., McClelland, J.W., Holmes, R.M., Zhulidov, A.V., Mull, K., Peterson, B.J., Striegl, R.G., Aiken, G.R., Gurtovaya, T.Y., 2007. Flux and age of dissolved organic carbon exported to the Arctic Ocean: a carbon isotopic study of the five largest arctic rivers. Glob. Biogeochem. Cycles 21, GB4011. https://doi.org/10.1029/2007GB002934.
Romanovsky, V.E., Smith, S.L., Christiansen, H.H., 2010. Permafrost thermal state in the polar Northern Hemisphere during the international polar year 2007–2009: a synthesis. Permafr. Periglac. Process. 21, 106–116. https://doi.org/10.1002/ppp.689.
Schaefer, K., Lantuit, H., Romanovsky, V.E., Schuur, E.A.G., Witt, R., 2014. The impact of the permafrost carbon feedback on global climate. Environ. Res. Lett. 9, 085003. https://doi.org/10.1088/1748-9326/9/8/085003.
Schuur, E.A.G., McGuire, A.D., Schaedel, C., Grosse, G., Harden, J.W., Hayes, D.J., Hugelius, G., Koven, C.D., Kuhry, P., Lawrence, D.M., Natali, S.M., Olefeldt, D., Romanovsky, V.E., Schaefer, K., Turetsky, M.R., Treat, C.C., Vonk, J.E., 2015. Climate change and the permafrost carbon feedback. Nature 520, 171–179. https://doi.org/10.1038/nature14338.
Shen, Y., Benner, R., Robbins, L.L., Wynn, J.G., 2016. Sources, distributions, and dynamics of dissolved organic matter in the Canada and Makarov basins. Front. Mar. Sci. 3, 1–20. https://doi.org/10.3389/fmars.2016.00198.
Shin, K.-H., Tanaka, N., 2004. Distribution of dissolved organic matter in the eastern Bering Sea, Chukchi Sea (Barrow Canyon) and Beaufort Sea. Geophys. Res. Lett. 31, L24304. https://doi.org/10.1029/2004GL021039.
Stedmon, C.A., Bro, R., 2008. Characterizing dissolved organic matter fluorescence with parallel factor analysis: a tutorial. Limnol. Oceanogr. Methods 6, 572–579.
Stedmon, C.A., Markager, S., 2005. Resolving the variability in dissolved organic matter fluorescence in a temperate estuary and its catchment using PARAFAC analysis. Limnol. Oceanogr. 50, 686–697.
Stedmon, C.A., Markager, S., Bro, R., 2003. Tracing dissolved organic matter in aquatic environments using a new approach to fluorescence spectroscopy. Mar. Chem. 82, 239–254. https://doi.org/10.1016/S0304-4203(03)00072-0.
Stedmon, C.A., Markager, S., Tranvik, L., Kronberg, L., Slätis, T., Martinsen, W., 2007. Photochemical production of ammonium and transformation of dissolved organic matter in the Baltic Sea. Mar. Chem. 104, 227–240. https://doi.org/10.1016/j.marchem.2006.11.005.
Stedmon, C.A., Amon, R.M.W., Rinehart, A.J., Walker, S.A., 2011a. The supply and characteristics of colored dissolved organic matter (CDOM) in the Arctic Ocean: Pan Arctic trends and differences. Mar. Chem. 124, 108–118. https://doi.org/10.1016/j.marchem.2010.12.007.
Stedmon, C.A., Thomas, D.N., Papadimitriou, S., Granskog, M.A., Dieckmann, G.S., 2011b. Using fluorescence to characterize dissolved organic matter in Antarctic sea ice brines. J. Geophys. Res. 116, G03027. https://doi.org/10.1029/2011JG001716.
Tanaka, K., Takesue, N., Nishioka, J., Kondo, Y., Ooki, A., Kuma, K., Hirawake, T., Yamashita, Y., 2016. The conservative behavior of dissolved organic carbon in surface waters of the southern Chukchi Sea, Arctic Ocean, during early summer. Sci. Rep. 6, 34123. https://doi.org/10.1038/srep34123.
Thomas, D.N., Kattner, G., Engbrodt, R., Giannelli, V., Kennedy, H., Haas, C., Dieckmann, G.S., 2001. Dissolved organic matter in Antarctic sea ice. Ann. Glaciol. 33, 297–303. https://doi.org/10.3189/172756401781818338.
Turetsky, M.R., Abbott, B.W., Jones, M.C., Anthony, K.W., Olefeldt, D., Schuur, E.A.G., Grosse, G., Kuhry, P., Hugelius, G., Koven, C., Lawrence, D.M., Gibson, C., Sannel, A.B.K., McGuire, A.D., 2020. Carbon release through abrupt permafrost thaw. Nat. Geosci. 13, 138–143. https://doi.org/10.1038/s41561-019-0526-0.
Walker, S.A., Amon, R.M.W., Stedmon, C.A., 2013. Variations in high-latitude riverine fluorescent dissolved organic matter: a comparison of large Arctic rivers. J. Geophys. Res. Biogeosci. 118, 1689–1702. https://doi.org/10.1002/2013JG002320.
Wheeler, P.A., Watkins, J.M., Hansing, R.L., 1997. Nutrients, organic carbon and organic nitrogen in the upper water column of the Arctic Ocean: implications for the sources of dissolved organic carbon. Deep-Sea Res. II Top. Stud. Oceanogr. 44, 1571–1592.
Wickland, K.P., Aiken, G.R., Butler, K., Dornblaser, M.M., Spencer, R.G.M., Striegl, R.G., 2012. Biodegradability of dissolved organic carbon in the Yukon River and its tributaries: seasonality and importance of inorganic nitrogen. Glob. Biogeochem. Cycles 26, GB0E03. https://doi.org/10.1029/2012GB004342.
Woodgate, R.A., Aagaard, K., 2005. Revising the Bering Strait freshwater flux into the Arctic Ocean. Geophys. Res. Lett. 32, L02602. https://doi.org/10.1029/2004GL021747.
Woodgate, R.A., Aagaard, K., Weingartner, T.J., 2005. Monthly temperature, salinity, and transport variability of the Bering Strait through flow. Geophys. Res. Lett. 32, L04601. https://doi.org/10.1029/2004GL021880.
Yamamoto-Kawai, M., Tanaka, N., Pivovarov, S., 2005. Freshwater and brine behaviors in the Arctic Ocean deduced from historical data of $\delta^{18}O$ and alkalinity (1929–2002 A.D.). J. Geophys. Res. 110, C10003. https://doi.org/10.1029/2004JC002793.
Yamamoto-Kawai, M., McLaughlin, F.A., Carmack, E.C., Nishino, S., Shimada, K., 2008. Freshwater budget of the Canada Basin, Arctic Ocean, from salinity, $\delta^{18}O$, and nutrients. J. Geophys. Res. 113, C01007. https://doi.org/10.1029/2006JC003858.
Yamamoto-Kawai, M., McLaughlin, F.A., Carmack, E.C., Nishino, S., Shimada, K., Kurita, N., 2009. Surface freshening of the Canada Basin, 2003–2007: river runoff versus sea ice meltwater. J. Geophys. Res. 114, C00A05. https://doi.org/10.1029/2008JC005000.
Yamashita, Y., Fichot, C.G., Shen, Y., Jaffé, R., Benner, R., 2015. Linkages among fluorescent dissolved organic matter, dissolved amino acids and lignin-derived phenols in a river-influenced ocean margin. Front. Mar. Sci. 2, 1–14. https://doi.org/10.3389/fmars.2015.00092.
Zhang, Y., Kang, S., Gao, T., Sprenger, M., Dou, T., Han, W., Zhang, Q., Sun, S., Du, W., Chen, P., Guo, J., Cui, X., Sillanpää, M., 2020. Dissolved organic carbon in Alaskan Arctic snow: concentrations, light-absorption properties, and bioavailability. Tellus Ser. B Chem. Phys. Meteorol. 72, 1–19. https://doi.org/10.1080/16000889.2020.1778968.